

# Neutral material around the B[e] supergiant star LHA 115-S 65 <sup>★</sup>

## An outflowing disk or a detached Keplerian rotating disk?

M. Kraus<sup>1</sup>, M. Borges Fernandes<sup>2,3</sup>, and F.X. de Araújo<sup>3\*\*</sup>

<sup>1</sup> Astronomický ústav, Akademie věd České republiky, Fričova 298, 251 65 Ondřejov, Czech Republic  
e-mail: kraus@sunstel.asu.cas.cz

<sup>2</sup> UMR 6525 H. Fizeau, Univ. Nice Sophia Antipolis, CNRS, Observatoire de la Côte d'Azur, Av. Copernic, F-06130 Grasse, France  
e-mail: Marcelo.Borges@obs-azur.fr

<sup>3</sup> Observatório Nacional, Rua General José Cristino 77, 20921-400 São Cristovão, Rio de Janeiro, Brazil  
e-mail: borges@on.br

Received ; accepted

### ABSTRACT

**Context.** B[e] supergiants are surrounded by large amounts of hydrogen neutral material, traced by the emission in the optical [O I] lines. This neutral material is most plausibly located within their dense, cool circumstellar disks, which are formed from the (probably non-spherically symmetric) wind material released by the star. Neither the formation mechanism nor the resulting structure and internal kinematics of these disks (or disk-like outflows) are well known. However, rapid rotation, lifting the material from the equatorial surface region, seems to play a fundamental role.

**Aims.** The B[e] supergiant LHA 115-S 65 (in short: S 65) in the Small Magellanic Cloud is one of the two most rapidly rotating B[e] stars known. Its almost edge-on orientation allows a detailed kinematical study of its optically thin forbidden emission lines. With a focus on the rather strong [O I] lines, we intend to test the two plausible disk scenarios: the outflowing and the Keplerian rotating disk.

**Methods.** Based on high- and low-resolution optical spectra, we investigate the density and temperature structure in those disk regions that are traced by the [O I] emission to constrain the disk sizes and mass fluxes needed to explain the observed [O I] line luminosities. In addition, we compute the emerging line profiles expected for either an outflowing disk or a Keplerian rotating disk, which can directly be compared to the observed profiles.

**Results.** Both disk scenarios deliver reasonably good fits to the line luminosities and profiles of the [O I] lines. Nevertheless, the Keplerian disk model seems to be the more realistic one, because it also agrees with the kinematics derived from the large number of additional lines in the spectrum. As additional support for the presence of a high-density, gaseous disk, the spectrum shows two very intense and clearly double-peaked [C III] lines. We discuss a possible disk-formation mechanism, and similarities between S 65 and the group of Luminous Blue Variables.

**Key words.** supergiants – stars: winds, outflows – stars: mass-loss – circumstellar matter – stars: individual: LHA 115-S 65

## 1. Introduction

B[e] supergiants in the Large and Small Magellanic Clouds (LMC and SMC), even though studied in great detail, are still far from being understood. A non-spherically symmetric wind is suggested by, e.g., polarimetric observations (Magalhães 1992; Magalhães et al. 2006; Melgarejo et al. 2001), and a circumstellar disk seems to be confirmed by their strong infrared excess emission due to circumstellar dust (e.g., Zickgraf et al. 1986) as well as by the emission of intense molecular bands like the CO first-overtone bands in the near infrared *K*-band spectra (McGregor et al. 1988a, 1988b, 1989; Morris et al. 1996), and TiO bands at optical wavelengths (Zickgraf et al. 1989). Based on the analysis of optical [O I] lines, it has recently been suggested that the disks around B[e] supergiants are neutral in hy-

drogen right from (or at least very close to) the stellar surface (Kraus & Borges Fernandes 2005; Kraus et al. 2006, 2007), so that molecules and dust are forming in the vicinity of the star. Indeed, for the LMC B[e] supergiant R 126, Kastner et al. (2006) found that the inner edge of the massive dusty disk must be located at  $\sim 360 R_*$ , which is about three times closer to the star than the value of  $\sim 1000 R_*$  formerly suggested by Zickgraf et al. (1985). The much closer inner edge of the dust disk requests that the [O I] emission must originate from distances between the surface of R 126 and  $\sim 360 R_*$ , which was confirmed by Kraus et al. (2007) considering a hydrogen neutral disk right from the stellar surface.

To guarantee that the disk material close to a luminous and hot supergiant star is neutral, the disk has to be massive (e.g., Kraus & Lamers 2003). Because the disks around supergiants cannot be pre-main sequence in origin, their formation must be linked to non-spherical (predominantly equatorial), high-density mass loss from the central star, either by some continuous steady material outflow, or by some mass-ejection event(s).

The formation of this anisotropic, high-density mass loss is assumed to be linked to rapid stellar rotation (e.g. Maeder & Meynet 2000; Kraus 2006). Especially rotation close to the crit-

<sup>★</sup> Based on observations done with the 1.52m and 2.2m telescope at the European Southern Observatory (La Silla, Chile) under the agreement with the Observatório Nacional-MCT (Brazil) and under programs 076.D-0609(A) and 080.A-9200(A)

<sup>\*\*</sup> We have to report with great sadness that our friend and colleague, Francisco Xavier de Araújo, deceased before this work could be finished

**Table 1.** Parameters of S 65. The rotation velocity was derived by Zickgraf (2000), the remaining parameters by Zickgraf et al. (1986).

$T_{\text{eff}}$ [K]	$R_*$ [ $R_{\odot}$ ]	$\log L_*/L_{\odot}$	$v \sin i$ [ $\text{km s}^{-1}$ ]	$E(B - V)$	inclination
17 000	81	5.7	$\sim 150$	$0.18 \pm 0.02$	$\pm$ edge-on

ical velocity could trigger the (rotationally induced) bi-stability mechanism (Lamers & Pauldrach 1991; Pelupessy et al. 2000; Curé 2004; Curé et al. 2005) as a plausible disk-formation scenario. And indeed, for at least four members of the B[e] supergiant group, the projected rotation speed (i.e.,  $v \sin i$ ) could be determined, showing that two of them are rotating at a substantial fraction (i.e., at least 75%) of their critical velocity. These are the SMC stars LHA 115-S 23 discussed in detail by Kraus et al. (2008) and LHA 115-S 65 (Zickgraf 2000). Whether all B[e] supergiants are rapidly rotating, is unknown however. The high-density wind observed around the other B[e] supergiants hides the central star, and the circumstellar material additionally contributes and pollutes the optical spectrum with a huge amount of emission lines. Consequently, the detection of uncontaminated photospheric lines, which would be appropriate for the determination of the projected stellar rotation velocity, is strongly hampered.

We study here the neutral material around the rapidly rotating SMC B[e] star LHA 115-S 65 (in short: S 65). The star S 65 is one of the four confirmed B[e] supergiants in the SMC. Its stellar parameters are summarized in Table 1 and have been determined by Zickgraf et al. (1986) and Zickgraf (2000). Our investigation makes use of the three optical [O I] emission lines detected in our spectra. We particularly aim to simultaneously reproduce the line luminosities and line profiles, to test the validity of any of the two most plausible B[e] supergiant disk scenarios: (i) an outflowing disk, which is neutral in hydrogen straight from the stellar surface, and (ii) a Keplerian rotating disk.

## 2. Observations and reductions

We obtained high-resolution optical spectra using the Fiber-fed Extended Range Optical Spectrograph (FEROS), and also low-resolution optical spectra using the Boller & Chivens spectrograph (B&C).

The FEROS spectra were obtained in three different years. The oldest one is from 1999 October 27, when the spectrograph was still attached to the 1.52-m telescope at the European Southern Observatory in La Silla (Chile), while the other spectra were taken on 2005 December 12, and 2007 October 3 and 4, after FEROS was moved to the 2.2-m telescope. FEROS is a bench-mounted Echelle spectrograph with fibers, where each one covers a sky area of  $2''$  of diameter. The wavelength coverage goes from  $3600 \text{ \AA}$  to  $9200 \text{ \AA}$  and the spectral resolution is  $R = 55\,000$  (in the region around  $6000 \text{ \AA}$ ). The spectra were obtained with exposure times of 7200 (1999), 900 (2005), and 900 (2007) seconds respectively. In 2005 and 2007, two exposures have been taken, which were then added for a better S/N ratio. The S/N ratio in the  $5500 \text{ \AA}$  region is approximately 90 (1999), 40 (2005), and 65 (2007). We adopted the complete automatic on-line reduction.

The low-resolution B&C spectrum was taken on 1999 October 28, with an exposure time of 900 seconds and a slit

width of  $4''$ . The instrumental setup employed provides a resolution of  $\sim 4.6 \text{ \AA}$  in the range of  $3800\text{--}8700 \text{ \AA}$ . The S/N ratio, in the  $5500 \text{ \AA}$  continuum region, is approximately 60. The B&C spectrum was reduced with standard IRAF<sup>1</sup> tasks, such as bias subtraction, flat-field normalization, and wavelength calibration. The absolute flux calibration was made using spectrophotometric standard stars cited in Hamuy et al. (1994).

## 3. Results

### 3.1. Spectral characteristics

A first detailed list of identified lines in the optical spectral range of S 65 has been compiled by Muratorio (1981). Later on, Zickgraf et al. (1986) re-observed S 65 at higher spectral resolution and with higher signal-to-noise ratio, and described their optical spectra in great detail. They found that the line spectrum showed many features in common with shell stars. These are the Balmer lines, which display a P Cygni profile of Beals' type III with a shell absorption reaching in most cases below the continuum, the Fe I emission lines with a central absorption core, and many additional singly ionized metal lines (like those from Cr II and Ti II, see Fig. 1) showing very narrow central absorption components which are nearly unshifted with respect to the emission component. For the typical B[e] supergiants, these well pronounced shell lines were thus interpreted by Zickgraf et al. (1986) as clear signatures for an edge-on orientation of the S 65 system. Further support for an edge-on orientation came from optical polarization measurements performed by Magalhães (1992) and Melgarejo et al. (2001). Follow-up observations with FEROS (Stahl 2001) showed no variability in the spectral lines of S 65, when compared to the spectra of earlier investigations. Indeed, comparing our own three spectra that cover a period of eight years to those of Zickgraf et al. (1986), as well as to the FEROS spectrum of Stahl (2001) that was obtained one year prior to our first spectrum, we could not find any significant difference in the individual line profiles, indicating that S 65 is not undergoing any severe variations. Nevertheless, before going into any modeling details, we will first provide a short description of the elements seen in our spectra and their line profiles. Due to the good quality of the spectra taken in 2007, we measured all the lines reported in this paper from these spectra. The spectra taken in 1999 and 2005 are used for a qualitative comparison.

Figure 1 covers some small portions of the optical spectrum of S 65. The numerous lines seen in these short wavelength ranges represent the richness in emission lines of the complete spectrum. A detailed investigation revealed only a few very weak photospheric absorption lines. Ten lines are from He I, which are all at least partly contaminated by or blended with circumstellar emission lines. This is shown for eight of them in Fig. 2. We also tentatively detected two lines from N II,  $\lambda\lambda$  3995 and 5679, and possibly one line from O II at  $\lambda$  3954.

The Balmer lines are present from H $\alpha$  up to H15. Figure 3 shows the line profiles of H $\alpha$  to H $\delta$ . The lowest Balmer lines display double-peaked profiles with a so-called violet-to-red ratio  $V/R < 1$  and a broad central absorption that extends below the continuum (except for H $\alpha$ , see Fig. 3). These line profiles are well-known from classical Be stars (or Be shell stars, e.g.,

<sup>1</sup> IRAF is distributed by the National Optical Astronomy Observatories, which are operated by the Association of Universities for Research in Astronomy, Inc., under cooperative agreement with the National Science Foundation.

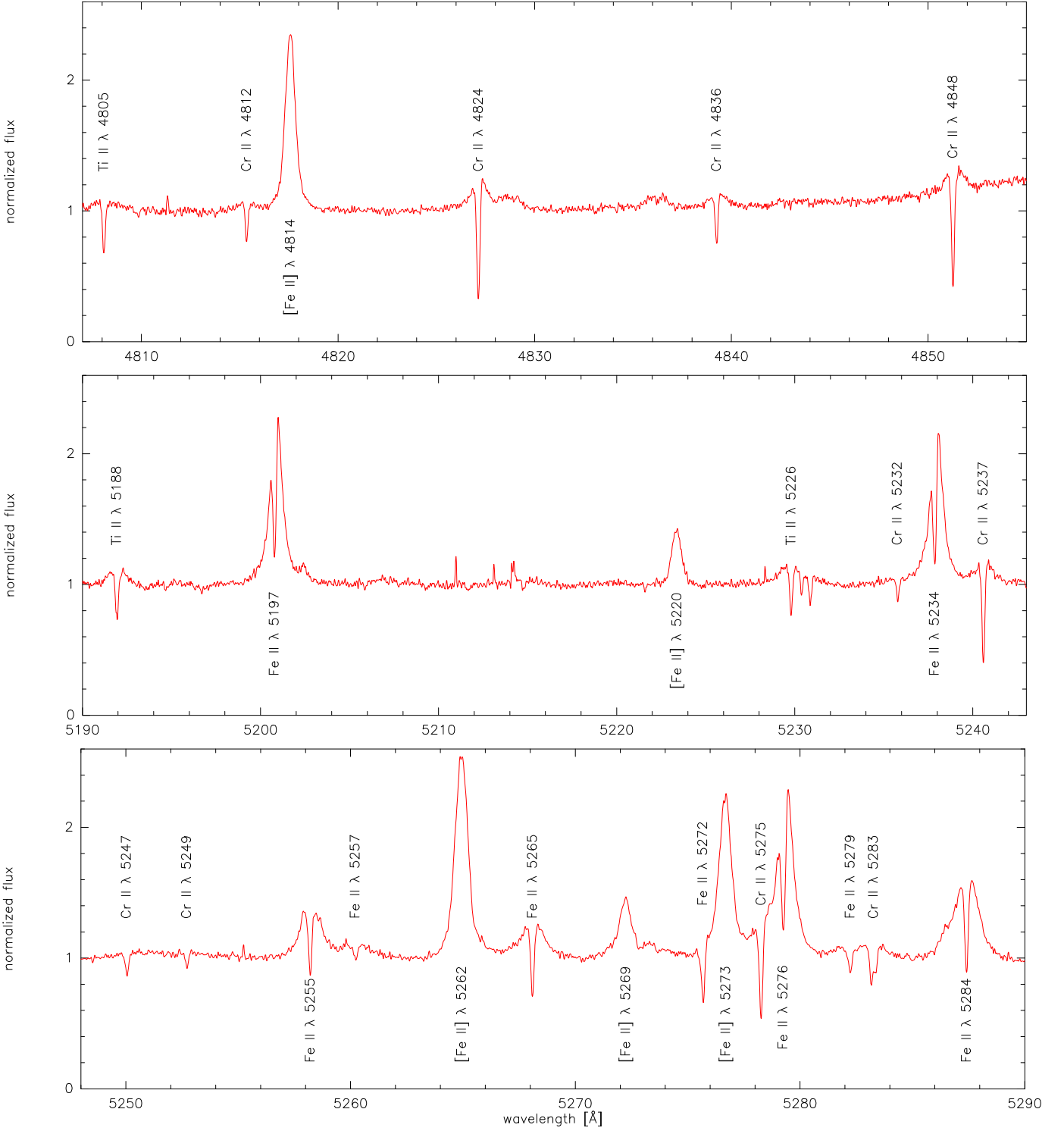


**Fig. 1.** Parts of our FEROS spectrum showing the two types of emission lines discussed in the text, i.e. the single-peaked emission lines of the forbidden transitions, and the permitted emission lines which all display a central or slightly blue-shifted sharp absorption component.

Hanuschik 2000) viewed edge-on. From  $H\delta$  on the shape of the lines turn into a P Cygni profile. The strength of the emission component thereby quickly decreases with higher quantum numbers, until for Balmer lines higher than  $H13$  only the absorption component remains. The absorption thereby consists of the P Cygni part and a shallow, but rather broad photospheric part,

as can be seen already for the  $H\delta$  line in Fig. 3. Also present are lines of the higher Paschen series, i.e., Pa10 up to Pa24, displaying P Cygni-type profiles. For the Paschen lines the absorption component also consists of a rather weak P Cygni absorption component, extending into the very shallow but much broader photospheric component.

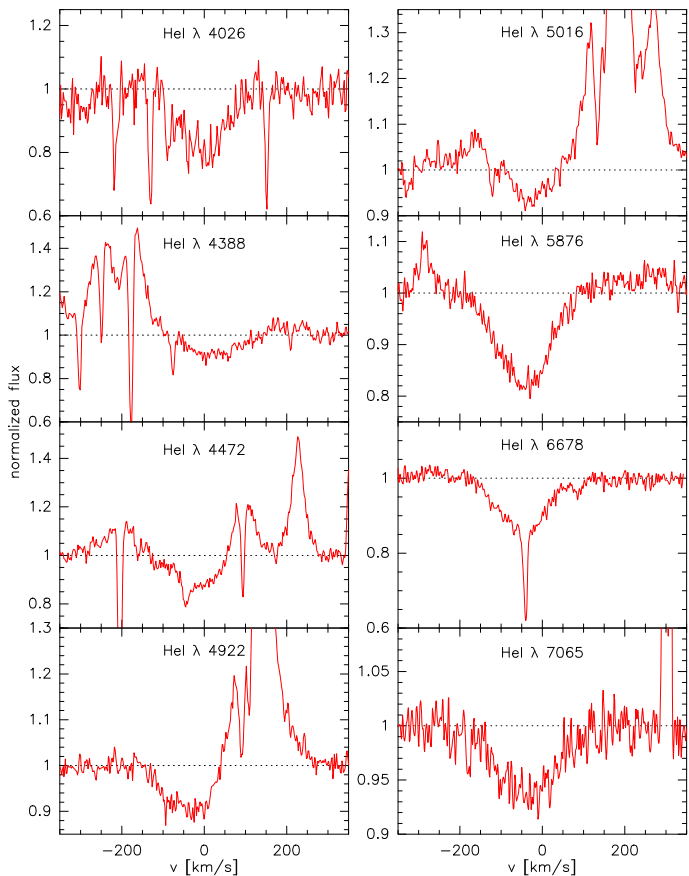


**Fig. 2.** Photospheric He I absorption lines. The lines are centered on the mean systemic velocity, which was determined as described in Sect. 3.2.

The huge number of additional lines seen in our spectra can basically be divided into two groups: single-peaked emission lines, and emission lines with a strong but very narrow, almost central absorption component reaching in most cases far below the continuum. The two types of profiles are nicely seen in the parts of the spectrum shown in Fig. 1.

All single-peaked emission lines are found to come from forbidden transitions. Most of the lines belong to [Fe II], but a few lines of [Cr II] and [Ni II], as well as one line from [Si II] are also visible. Additional lines (but blended or very weak) from [Ti II], [Mg I], [Mg II], and [Ni I] might be present. We also found a few very weak emission lines from permitted transitions; they belong to C I and Ni.

The group of emission lines with the strong central absorption contains by far the largest number of lines. We could identify more than 230 lines, most of them belonging to transitions of Fe II, Cr II, and Ti II. But few lines from other elements like Mn II, Mg I, Ca II, Si II, and Fe I were also found. The strong, sharp, and almost central absorption components indicate high-density absorbing material along the line of sight with a rather small radial velocity component. As mentioned earlier, the line shapes recall those seen in Be shell stars or Be disks viewed edge-on. It is therefore reasonable to assume that S 65 is surrounded by a high-density disk or ring structure viewed edge-on, as suggested by Zickgraf et al. (1986).

Interestingly, the spectrum shows prominent emission of the [O I] lines as well as of the [Ca II] lines. However, their line profiles do not fit into the groups described above. Instead, their

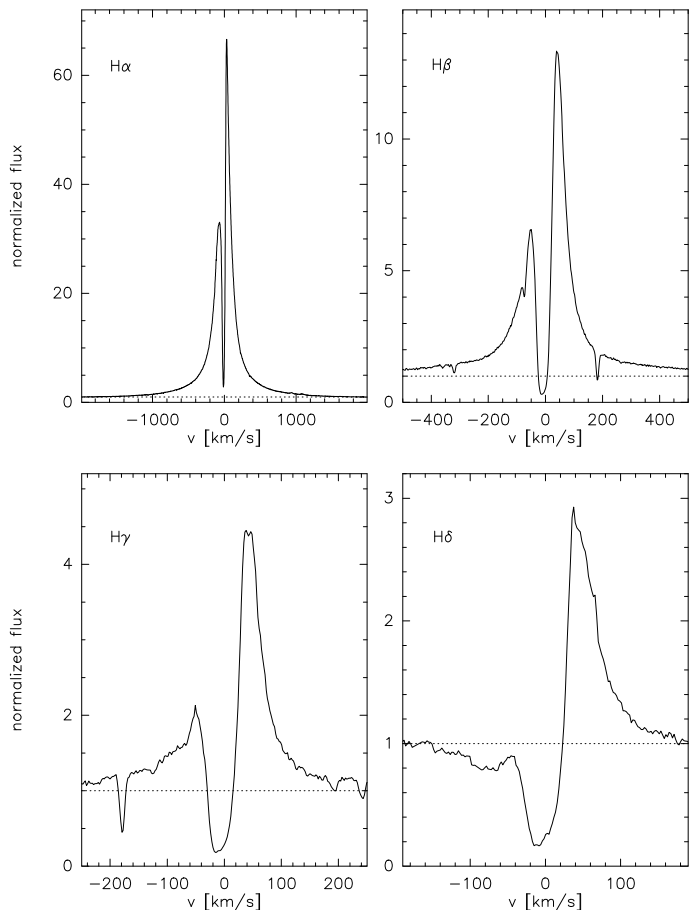


**Fig. 3.** Balmer line profiles showing a variation in shape. The lines are centered on the mean systemic velocity of S 65, which was determined as described in Sect. 3.2.

profiles show a clear double-peaked structure (see Fig. 4). This type of profile is usually interpreted with Keplerian rotation in a circumstellar disk.

### 3.2. Systemic and projected rotational velocity of S 65

The strong pollution of the photospheric He I absorption lines by adjacent emission from the circumstellar material (Fig. 2) makes it impossible to accurately determine their line centers. Therefore we need to rely on the emission lines to derive the systemic velocity. As mentioned in the previous section, the permitted lines all show a sharp central absorption. The slight asymmetry seen in most of these line profiles in form of a slightly stronger red emission compared to the blue emission peak hampers a proper determination of their line centers. In addition, this asymmetry indicates that the central absorption components seem to be in many cases slightly blue-shifted. Hence they do not mirror the systemic velocity of the system, but only the dynamics along the line-of-sight through the high-density disk (see Sect. 4). The only reasonable set of lines for a proper systemic velocity determination is thus provided by the optically thin, single-peaked and symmetric profiles of the forbidden emission lines. From the whole sample of forbidden lines detected, we restricted our selection to the strongest and unblended ones and measured their central wavelengths by fitting Gaussian profiles using IRAF. From the difference between the measured and the laboratory wavelengths we computed the radial velocity, which

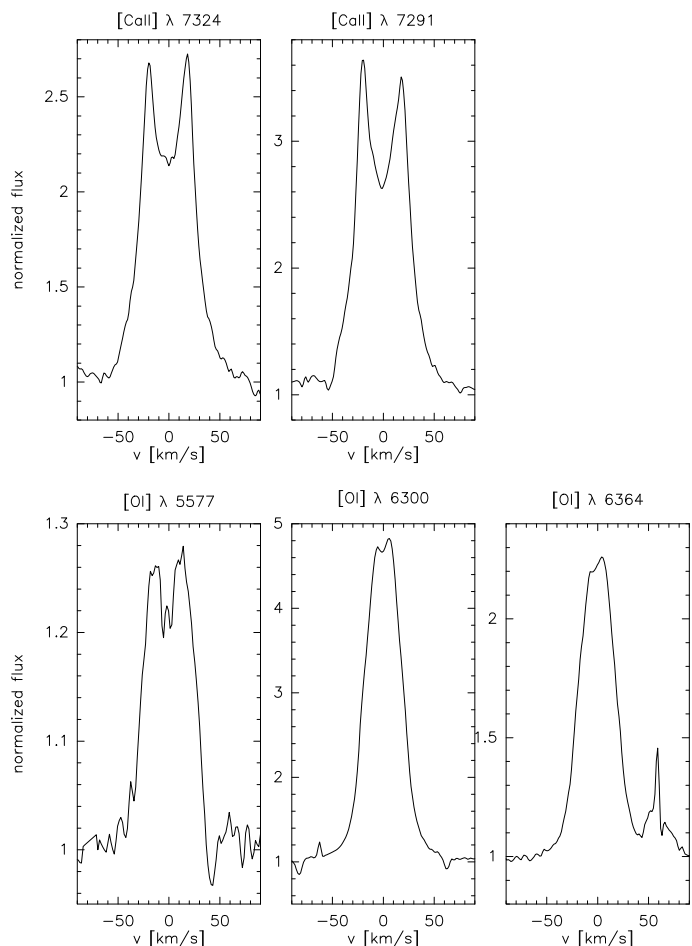


**Fig. 4.** Line profiles of the [CaII] (top) and [OI] lines (bottom). The lines are centered on the mean systemic velocity of S 65, which was determined as described in Sect. 3.2.

is plotted in Fig. 5. The mean radial (heliocentric) velocity we found is  $v = (+189.23 \pm 0.74) \text{ km s}^{-1}$ , which can be interpreted as the systemic velocity of S 65. Our mean value agrees very well with the value of  $(+191 \pm 4) \text{ km s}^{-1}$  derived by Zickgraf et al. (1986), and also fairly well with the values of  $+184 \text{ km s}^{-1}$ , and  $(+193 \pm 6) \text{ km s}^{-1}$  obtained in earlier investigations by Feast et al. (1960) and Maurice (1976), respectively, when we account for the lower resolutions and lower S/N values of those older spectra. Therefore we consider our value as reasonably good and use it throughout the paper to correct the measured velocities with respect to the systemic velocity, as done, e.g., for the line profile plots in Figs. 2 to 4.

We emphasize that the HeI absorption lines cannot be formed in the (polar) wind of S 65, because the effective temperature of the star (and hence the wind temperature) is too low to keep helium ionized beyond the photosphere. Therefore they can be considered as of pure photospheric origin. The width of these HeI lines and also of the (shallow) photospheric absorption components of the Balmer and Paschen lines cannot be caused by broadening mechanisms like macroturbulence and pressure broadening alone. These two effects in the atmospheres of B-type supergiants typically add up to a few tens of  $\text{km s}^{-1}$ , only. Instead, the broad and roundish shape of the lines suggests that they are predominantly broadened by the possibly high rotation of the star, as suggested by Zickgraf (2000).

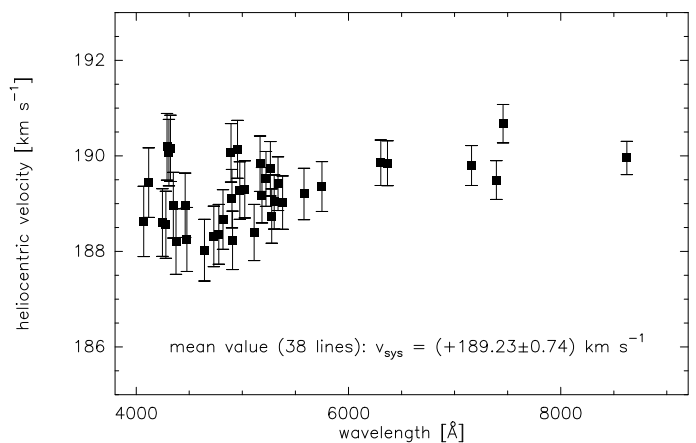


**Fig. 5.** Radial (heliocentric) velocity of S 65 derived from the strong and symmetric non-blended single-peaked forbidden emission lines.

**Table 2.** Measured *HWHM* and derived  $v \sin i$  values of the three HeI lines in Fig. 6.

Line	<i>HWHM</i> [Å]	$v \sin i$ [ $\text{km s}^{-1}$ ]
HeI 4922	$1.81 \pm 0.10$	$141.8 \pm 7.4$
HeI 5876	$2.37 \pm 0.09$	$155.2 \pm 6.0$
HeI 7065	$2.91 \pm 0.14$	$158.1 \pm 7.5$

Our derived systemic velocity allows us to determine the proper line centers of the HeI lines. Inspection of these lines (see Fig. 2) shows that the blue parts of at least three lines (HeI  $\lambda\lambda$  4922, 5876, and 7065) seem to be uncontaminated, nicely displaying the roundish profile shape as expected in rotationally broadened photospheric absorption lines. The blue half of these three HeI lines are shown in Fig. 6. Their wings extend to Doppler velocities of about  $150\text{--}180 \text{ km s}^{-1}$ . A comparable Doppler velocity is also seen in the shallow photospheric absorption components of the hydrogen lines (see, e.g., the line profile of H $\delta$  in Fig. 3).

We measured the half-width at half-maximum (*HWHM*) values of these three HeI lines in Fig. 6. From those values, the projected rotation velocity,  $v \sin i$ , can be computed under the assumption of a stellar rotation profile as derived, e.g., by Gray (1976) and with a limb-darkening coefficient of 0.6. The measured *HWHM* and the derived  $v \sin i$  values are listed in Table 2. Compared to the value of  $\sim 150 \text{ km s}^{-1}$  obtained by Zickgraf (2000), our values excellently agree. Given that the HeI  $\lambda$ 5876 line is the strongest in our sample, we consider our value of  $(155.2 \pm 6.0) \text{ km s}^{-1}$  derived from that line as a reasonably good value for the projected rotation velocity of S 65.

We note however that this value might be an underestimation of the real projected stellar rotation velocity. Expressed in terms of the critical rotation velocity, the derived value of  $\sim 155 \text{ km s}^{-1}$  corresponds to  $v \sin i / v_{\text{crit}} \simeq 0.75$ . For stars rotating so rapidly Townsend et al. (2004) have shown that the *HWHM* method is not reliable anymore to derive the correct projected stellar rotation velocity, because the effects of gravitational darkening influence the photospheric absorption lines in a way that their line width does not increase anymore for  $v \sin i / v_{\text{crit}} > 0.75$ . This means that even if the star would rotate at a velocity close to the critical one, the measured *HWHM* would only imply a value of

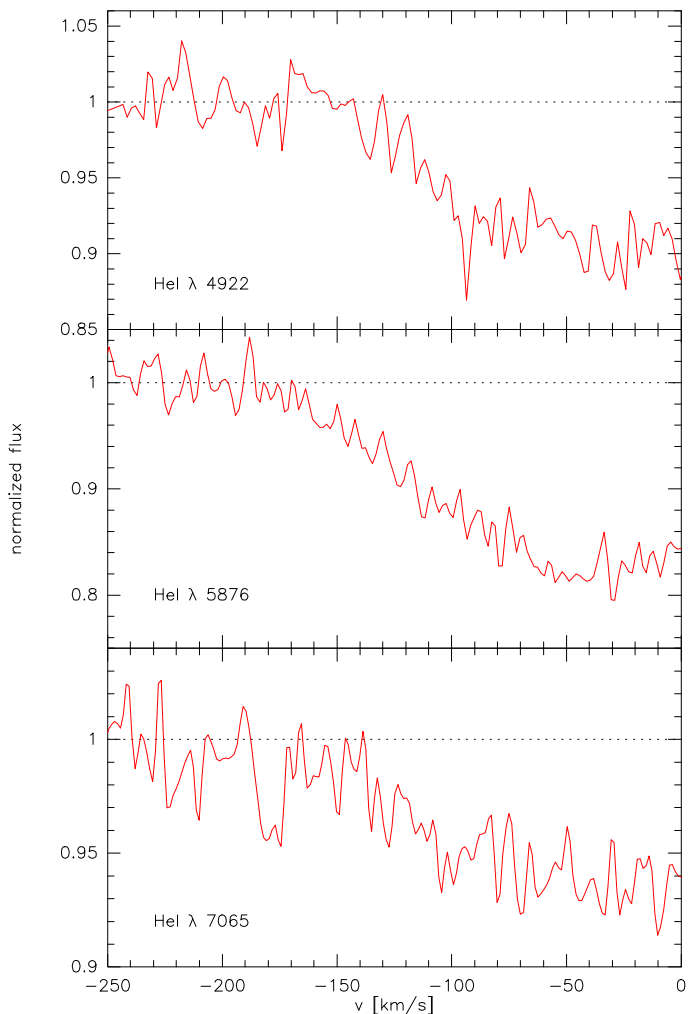


**Fig. 6.** Untaminated blue parts of three He I lines from Fig. 2.

$v \sin i / v_{\text{crit}} \approx 0.75$ . Our value can thus only be considered as a lower limit to the real projected stellar rotation of S 65.

### 3.3. The [O I] lines

In the remaining part of this section we concentrate on the [O I] emission lines arising in the circumstellar material of S 65, aiming to find a reasonable scenario to explain the observed [O I] line luminosities and profiles.

The FEROS spectrum displays three [O I] lines (see Fig. 4). They originate from transitions within the five lowest energy levels of neutral oxygen. Based on the flux-calibrated (but low-resolution) B&C spectrum, we can derive the line luminosities of the [O I] lines. Zickgraf et al. (1986) determined an interstellar extinction towards S 65 of  $E(B - V) = 0.18 \pm 0.02$  (see Table 1). We used this value and applied the interstellar extinction curve of the SMC of Prévot et al. (1984) to deredden the B&C spectrum. With the calibrated dereddened continuum and a distance modulus of  $\mu = 18.93 \pm 0.02$  for the SMC (Keller & Wood 2006), we then calculated the observed luminosities in the [O I] lines (see Table 3) from the measured equivalent widths in the FEROS spectrum. The errors in line luminosities are about 10%, following from the uncertainties in equivalent width measurements, interstellar extinction, and distance.

**Table 3.** Velocities obtained from the peak separation and  $FWHM$  values and extracted line luminosities of the [O I] lines. The errors in the line luminosities are on the order of 10%.

$\lambda$ [Å]	$v_{\text{peaks}}$ [km s <sup>-1</sup> ]	$v_{FWHM}$ [km s <sup>-1</sup> ]	$L_{\text{line}}$ [erg s <sup>-1</sup> ]
5577	$44 \pm 2$	$56 \pm 2$	$8.28 \times 10^{33}$
6300	$24 \pm 2$	$43 \pm 2$	$8.46 \times 10^{34}$
6364	$24 \pm 2$	$42 \pm 2$	$2.93 \times 10^{34}$

The major advantage in using forbidden emission lines is that because they are optically thin, their line profiles contain the full velocity information of their formation region. The observed line profiles of the [O I]  $\lambda$  6300 and 6364 lines are more or less identical. This is clear, because both lines arise from the same upper level, which means that they are formed in the same region in terms of density and temperature. While both lines show only a slight indication of a double-peaked profile, this double-peak structure is more pronounced in the [O I]  $\lambda$  5577 line, and the measured peak velocities and  $FWHM$  values of all three lines are listed in Table 3. This latter line arises from a higher energy level. Because the levels from which the forbidden lines originate are purely collisionally excited, the [O I]  $\lambda$  5577 line must be formed in regions of a higher density and/or higher temperature. This could indicate that the  $\lambda$  5577 line originates from regions closer to the star. In combination with the broader  $FWHM$  as well as the broader peak separation, which mirror a higher velocity within the  $\lambda$  5577 line-forming region, this qualitative analysis might already hint at a Keplerian disk rather than a pure outflowing disk.

However, based purely on the appearance of a double-peaked structure of the line profiles, it is not possible to discriminate whether the [O I] line-forming region is located in a Keplerian rotating disk or in an outflowing disk, because both scenarios, when viewed edge-on, result in identical, double-peaked line profiles. Reliable conclusions about the real kinematical nature of the [O I] line-forming region can thus only be drawn from a proper and simultaneous modeling of both line profiles, from which the kinematical information is taken and the line luminosities, delivering the information about the density and temperature. This is done below for the two competing scenarios: the outflowing and the Keplerian rotating disk model.

#### 3.3.1. Outflowing disk model

Not much is known in the literature concerning the structure and shape of the disks around B[e] supergiants, and there is an ongoing debate whether they are Keplerian rotating, or outflowing in nature (see, e.g., Porter 2003; Kraus et al. 2007). From a statistical point of view (based on low number statistics though), it seems that the disks must be rather thick, with an opening angle of about  $\alpha \approx 20^\circ$  (Zickgraf 1989), which is 4–5 times larger than the opening angle of classical Be stars (see, e.g., Porter & Rivinius 2003).

Another key question is related to the ionization structure in the disk. Oxygen has about the same ionization potential as hydrogen. The detection of emission lines from neutral oxygen thus means that these lines must be generated within a region in which hydrogen is predominantly neutral as well. Free electrons are (besides the less efficient, but nevertheless important, neutral hydrogen atoms) the main collision partners to excite the lowest energy levels in neutral oxygen, from which the forbidden emis-



sion lines arise. We follow the approach of Kraus et al. (2007) and introduce the parameter  $q_e$  as the ionization fraction, defined by  $n_e = q_e n_H$ , with  $q_e = q_{\text{Metals}} + q_{\text{H}^+}$ , and the electron and hydrogen particle densities,  $n_e$  and  $n_H$ , respectively. Assuming that all elements with an ionization potential lower than that of hydrogen and oxygen are fully ionized delivers an upper limit of  $q_{\text{Metals}} < 9.5 \times 10^{-5}$ . For this, we used an SMC metallicity of 20% solar (see, e.g., Dufton et al. 2005), and solar abundance values for the metals from Grevesse & Sauval (1998). This very low value obtained from the metals means that if hydrogen is ionized by only 1%, it still provides the dominant quantity of free electrons. Because we do not know the amounts of ionized hydrogen and ionized metals within the [O I] line-forming region, we keep  $q_e$  as a free parameter at first.

An additional important parameter is the electron temperature in the [O I] line-forming region. It should be lower than the hydrogen ionization temperature, and higher than the molecule dissociation threshold, below which atomic oxygen is bound into CO molecules. While the former restriction defines the maximum temperature at about 10 000 K, the latter corresponds to a minimum temperature of roughly 5000 K, which is the dissociation temperature of CO.

To calculate the population of the five lowest energy levels in atomic oxygen, we need to take into account collisions from both free electrons and neutral hydrogen atoms. The collision parameters for excitation by neutral hydrogen atoms are taken from Störzer & Hollenbach (2000), those for excitation by free electrons from Mendoza (1983), and atomic parameters are from Wiese et al. (1966) and Kafatos & Lynch (1980). We calculate the level population by solving the statistical equilibrium equations in a 5-level atom. Forbidden emission lines are optically thin so that no complicated radiation transfer needs to be solved. Instead, the emissivity at any location  $r$  in the disk is simply given by  $j_{n,m}(r) = h\nu_{n,m}n_n(r)A_{n,m}$  where  $n_n(r)$  is the level population of the upper level, and  $A_{n,m}$  is the Einstein coefficient of spontaneous emission. The line luminosities finally follow from integration of the emissivities over the emitting disk volume.

Next, we can restrict the valid ranges in electron temperature and ionization fraction,  $q_e$ , within the [O I] line-forming regions in the disk of S 65. Because two of the observed [O I] lines ( $\lambda 6300$  and  $\lambda 6364$ ) originate from the same upper level, their line ratio is determined by pure quantum mechanics and does not depend on density and temperature. The  $\lambda 5577$  line, however, originates from a higher energy level. A sufficiently strong population of this level thus severely depends on the density of the collision partners as well as on temperature. Any ratio with this line is therefore an ideal tracer for the density and temperature, and we concentrate on the  $\lambda 6300/\lambda 5577$  line ratio below to constrain these two parameters.

In the top panel of Fig. 7 we show the  $\lambda 6300/\lambda 5577$  line ratio as a function of the ionization fraction,  $q_e$ , and for different (constant) values of the electron temperature. The calculations performed with the outflowing disk model request the knowledge of the mass flux. For simplicity, we assume a latitude independent mass flux within the disk-forming wind region, i.e.,  $F_m(\theta) = F_{m,\text{Disk}} = \text{const.}$  for all latitudes in the range  $[90^\circ - (\alpha/2)] < \theta < [90^\circ + (\alpha/2)]$ . We also assume the wind to have a constant outflow velocity,  $v_{\text{out}}$ , delivering the density parameter,  $F_{m,\text{Disk}}/v_{\text{out}}$ , as one free input parameter. With this density parameter we can calculate the hydrogen density at the inner edge of the disk (here: at the stellar surface) and consequently also the radial density distribution  $n_H(r) \sim (F_{m,\text{Disk}}/v_{\text{out}}) r^{-2}$  resulting from the application of the equation of mass continuity. Due to the radially decreasing density, the [O I] line luminosities

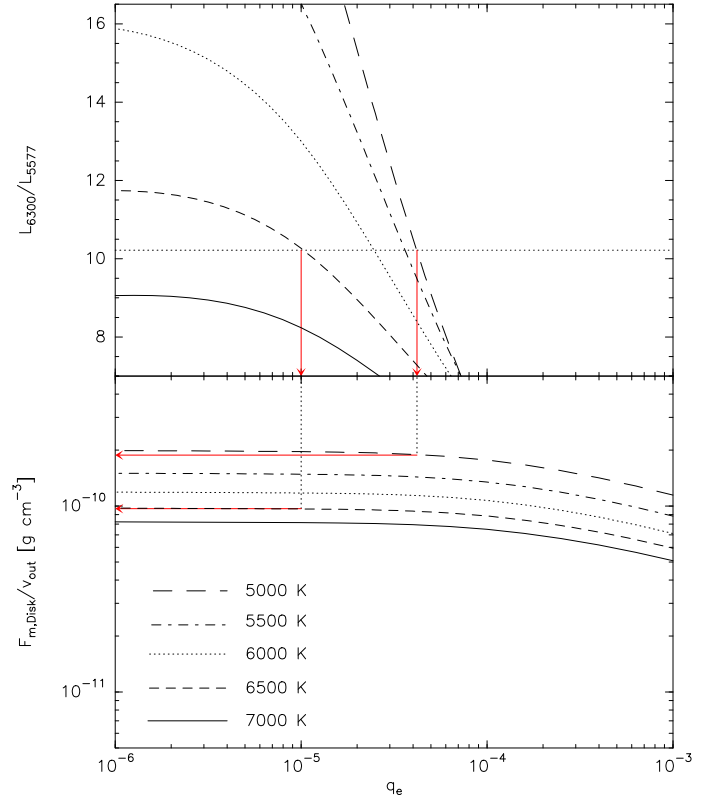


**Fig. 7.** *Top panel:* Theoretical line ratios as function of  $q_e$  at fixed temperature. The intersection with the observed value (dotted horizontal line) defines the valid ( $q_e, T_e$ ) range (arrows). *Bottom panel:* Density parameter as function of  $q_e$  at fixed temperature. The valid ( $q_e, T_e$ ) range (dotted vertical lines) delivers the range in density parameters (arrows).

ties saturate at a certain distance. This saturation value should agree with the observed line luminosities. We thus varied the density parameter,  $F_{m,\text{Disk}}/v_{\text{out}}$ , for a fixed pair of ( $T_e, q_e$ ) values, until the observed  $\lambda 6300$  line luminosity was reproduced. The line ratio with the  $\lambda 5577$  line resulting from these calculations defines one single point in the diagram shown in the top panel of Fig. 7. This procedure was repeated until a sufficiently large coverage of the ( $T_e, q_e$ ) parameter space was obtained. We then compared the theoretical results to the observed line ratio, which is shown as the dotted line. Based on the discussion above concerning the valid range in temperatures, the curve for  $T_e = 5000$  K can be considered as the lower temperature limit, resulting in a *strict upper limit* for the ionization fraction in the disk of S 65 of  $q_{e,\text{max}} = 4.2 \times 10^{-5}$ . This means that the [O I] line-forming region must indeed be neutral in hydrogen, with  $q_{\text{H}^+} \lesssim q_{e,\text{max}} = 4.2 \times 10^{-5}$ . For a temperature of 7000 K, the observed line ratio cannot be reproduced. The maximum temperature in the [O I] line-forming region must thus lie between 6500 K and 7000 K. Since the plot in the top panel of Fig. 7 indicates that a higher temperature would imply a lower degree of ionization, it is reasonable to assume that the most plausible range in temperature is  $T_e \approx 5500 \dots 6500$  K, delivering a disk ionization fraction of  $q_e \approx (1 \dots 4) \times 10^{-5}$ .

In the bottom panel of Fig. 7 we plot the density parameter, used for the line luminosity fit of the  $\lambda 6300$  line and the resulting line ratio as shown in the top panel, as a function of  $q_e$  and for the different temperature values. In the part of the diagram where

the ionization fraction is high, the density parameter shows (for a given temperature) a power-law dependence with  $q_e$ . This means that for decreasing ionization fraction the input density has to be increased to compensate for the otherwise decreasing number of free electrons. On the other hand, below an ionization fraction of a few times  $10^{-5}$ , the input density parameters stagnate. This means that for ionization fractions  $q_e \lesssim 10^{-4}$  collisions with neutral H atoms start to become important. For further decreasing ionization fraction they even dominate the level population process, because at very low ionization the neutral particles are finally numerous enough for efficient collisional level population. From the narrow range of valid temperatures and ionization fraction values, the range in density parameter is confined to  $F_{m,\text{Disk}}/v_{\text{out}} \simeq (1 \dots 2) \times 10^{-10} \text{ g cm}^{-3}$ .

These calculations, even though they are performed under several simplifying assumptions, show that the [OI] line-forming region is well constrained in temperature and density. And the increase of the individual line luminosities with distance from the star and their saturation is shown for all three [OI] lines in the upper panel of Fig. 8. These computations exemplify the case of a constant temperature of 6000 K and resulting values of  $2.49 \times 10^{-5}$  and  $1.16 \times 10^{-10} \text{ g cm}^{-3}$  for the ionization fraction and density parameter, respectively. The arrows to the right indicate the observed line luminosity values with their errors indicated by the vertical bars.

The luminosity saturation of the  $\lambda 5577$  line occurs at a distance of about  $20 - 30 R_*$ , and therefore rather close to the star, while saturation in the luminosities of the other two lines happens only at distances beyond  $\sim 400 R_*$ , i.e., at least 10 times further out and therefore in regions in which the density is at least 100 times lower. To check the influence of the disk temperature on these results we also calculated the line luminosities for a disk with 6500 K and 5500 K. A lower (higher) temperature requires slightly higher (lower) values for the ionization fraction and density parameter (see Fig. 7). The corresponding curves for the increases in line luminosities are, however, hardly affected, and the saturations of the [OI] lines happen at the same distances. What remains to check is whether this outflowing disk scenario is a reasonable model to explain the observed line profiles.

Because the lines are formed in different disk regions, their profiles mirror the kinematics at these different distances from the star. The double-peaked profile of the  $\lambda 5577$  line might be interpreted with an outflow velocity of about  $v_{\text{out}} \simeq 22 \text{ km s}^{-1}$ , obtained from the separation between the blue edge of the blue and the red edge of the red peak (Table 3). The broader wings of the line require an additional Gaussian-shaped velocity component, i.e., additional to the thermal velocity plus spectral resolution, which result in a Gaussian velocity component of about  $6 \text{ km s}^{-1}$ . This additional Gaussian velocity could be ascribed to some turbulent motion of the gas and is found to be on the order of  $v_{\text{turb}} \simeq 8 \text{ km s}^{-1}$ . The resulting fit to the  $\lambda 5577$  line is shown as the dashed line in the bottom panel of Fig. 8.

For the other two [OI] lines ( $\lambda 6300$  and  $\lambda 6364$ ) this model does not hold (dotted lines in the lower panel of Fig. 8). Instead, the observed profiles are much narrower and the peak-separation is less pronounced than in the  $\lambda 5577$  line. Nevertheless, we find good fits to these line profiles, too, if we assume an outflow velocity of only  $16 \text{ km s}^{-1}$ , but a turbulent velocity of  $11 \text{ km s}^{-1}$  (dashed lines in the lower panel of Fig. 8). This would imply that because these lines are generated much further out, the outflow velocity of the disk would have slightly slowed down, with a simultaneous slight increase of the turbulent velocity.

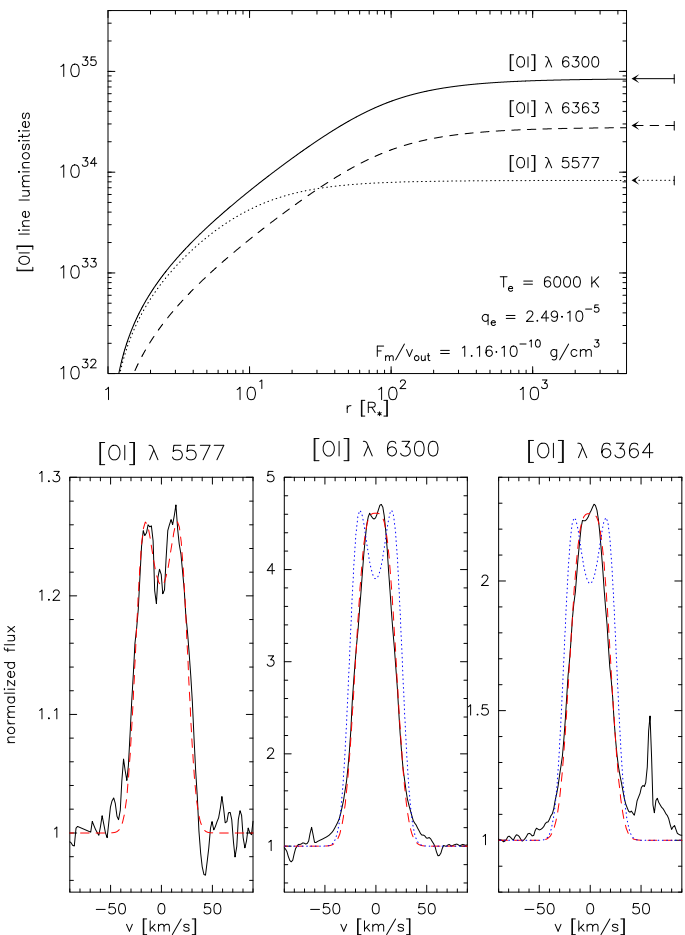


**Fig. 8.** *Top panel:* Predicted [OI] line luminosities from within a radius  $r$  in the outflowing disk scenario. The arrows to the right indicate the observed values. *Bottom panel:* Fits to the line profiles. The dotted profiles fitted to the  $\lambda 6300$  and  $\lambda 6364$  lines are obtained for the same constant outflow velocity as the  $\lambda 5577$  line; the dashed lines in all profiles show our best fit.

### 3.3.2. Keplerian rotating disk or ring

The decrease in peak separation seen in the [OI] lines from a higher value at higher densities, i.e., closer to the star, to a lower value further out, could be a clear indication for Keplerian rotation. Therefore we now calculate the [OI] line luminosities and the profiles with a Keplerian rotating disk model. To translate the rotation velocities as inferred from the peak separations of the line profiles into radial distances, we need to know the current mass of the star. Its effective temperature and luminosity, when compared to evolutionary tracks of rotating (Meynet & Maeder 2005) and non-rotating stars at SMC metallicity (Charbonnel et al. 1993), place S 65 within the HR diagram to a region in agreement with a post-main sequence evolutionary phase of a star with an initial mass in the range  $35 - 40 M_{\odot}$ , and we assume a current mass of  $\sim 35 M_{\odot}$ .

The peak separations of the  $\lambda 6300$  and  $\lambda 6364$  lines deliver a minimum rotation velocity of about  $5 \dots 6 \text{ km s}^{-1}$ , which sets the outer edge of the [OI] line emission region to about  $R_{\text{out}} \simeq 3000 R_*$ . The  $\lambda 5577$  line, which is created much closer to the star, thus delivers the velocity information from the inner parts of the Keplerian rotating disk. Due to the extended region over which the [OI] line is generated, its peak separation does not



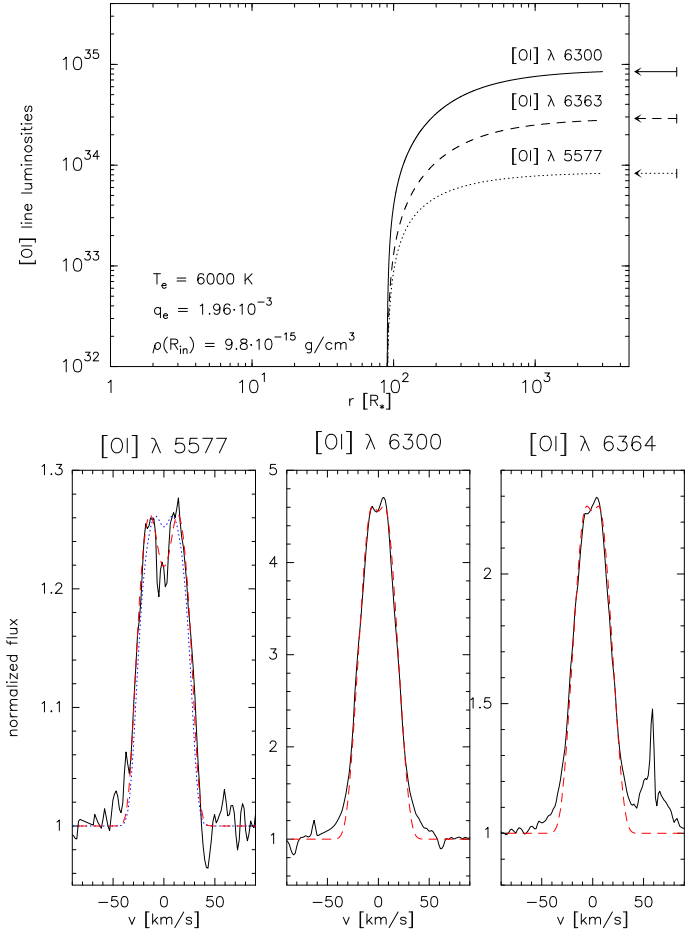


**Fig. 9.** *Top panel:* Same as Fig. 8 but for the Keplerian rotating disk scenario. *Bottom panel:* Fits to the line profiles. The dotted profile fitted to the  $\lambda 5577$  line is for a purely rotating disk model; the dashed lines in all profiles account for our best-fit model.

reflect the rotation velocity at the inner edge of the disk, but the velocity at the distance where the bulk of emission in this line is created. The distance at which a rotation velocity of  $22 \text{ km s}^{-1}$  is achieved is at about  $170 R_*$ . The *FWHM* of about  $56 \text{ km s}^{-1}$  implies a rotation velocity of  $28 \text{ km s}^{-1}$  and a distance of  $105 R_*$  at which already some substantial fraction of the emission must be generated. The real inner edge of the disk must be slightly closer to the star though, and our test calculations revealed a most likely distance of  $R_{\text{in}} \approx 90 R_*$  delivering a maximum rotation velocity to the profile of the  $\lambda 5577$  line of  $v_{\text{rot,max}} \approx 30 \text{ km s}^{-1}$ .

While the velocity distribution in a Keplerian rotating disk is well known, the situation is far less clear for the radial density distribution within this disk. For simplicity we adopt a  $r^{-2}$  behavior of the density distribution. A justification for this choice might be given by the request that the disk must have been formed from an outflow or ejection process obeying the mass continuity relation. In addition, a  $r^{-2}$  density distribution is also known to settle over large regions within the so-called wind-wind interaction regions (e.g., Steffen & Schönberner 2003). However, different power-law density distributions, as, e.g., found in Keplerian disks around pre-main sequence stars, cannot be excluded.

For a first guess of the ionization fraction and density parameter at the inner edge of the disk, we calculate the line luminosities and the  $\lambda 6300/\lambda 5577$  line ratio for the same range

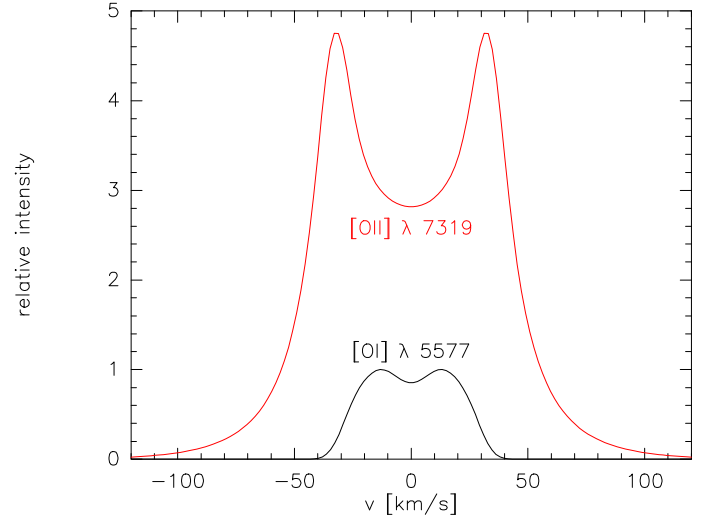


**Fig. 10.** Expected strength and shape of the [O II]  $\lambda 7319$  line in the Keplerian rotating disk scenario.

of constant temperatures (5000 K to 7000 K) and a disk extending from  $\sim 90 R_*$  to  $\sim 3000 R_*$ . Proceeding as in Sect. 3.3.1 we find the following plausible ranges for the disk parameters:  $q_e \approx (1.3 \dots 3.6) \times 10^{-3}$  and  $F_{\text{m,Disk}}/v_{\text{out}} \approx (0.5 \dots 1.0) \times 10^{-10} \text{ g cm}^{-3}$ , or, when expressed in terms of the density,  $\rho$ , at the inner edge of the disk,  $\rho(R_{\text{in}}) \approx (0.6 \dots 1.2) \times 10^{-14} \text{ g cm}^{-3}$ .

The results of the line luminosity calculations performed for a constant temperature of  $T_e = 6000 \text{ K}$  are shown in the top panel of Fig. 9. They indicate that for a Keplerian rotating disk the ionization fraction,  $q_e$ , must be higher by about a factor of 100 compared to the one found for the outflowing disk model. This trend is clear, because the line formation is now forced to happen at much larger distances from the star, where the O I density is generally much lower. Therefore, a higher number of collision partners (i.e., free electrons) is necessary to produce the same line luminosity. Nevertheless, even with this much higher ionization fraction, the disk can still be considered as being neutral in hydrogen ( $q_{\text{H}^+} < 2 \times 10^{-3}$ ).

The calculated profile fits to the [O I] lines, resulting from our Keplerian disk model, are shown in the bottom panel of Fig. 9. It is obvious that the  $\lambda 6300$  and  $\lambda 6364$  lines can be fitted quite well, as shown by our dashed-line fits to these two lines. However, the same model fails (indicated by the dotted line) to reproduce the  $\lambda 5577$  line profile. Although the Keplerian disk model results in a slightly double-peaked profile for that line as well, its shape is nevertheless significantly different from the observed one. Especially the inter-peak strength is strongly overestimated. To obtain a better reproduction of the  $\lambda 5577$  line profile, we thus have to assume that the material at the inner edge of the disk is not purely rotating, but an additional kinematical component, resulting in a double-peaked line profile, must exist as well. Because our investigations in the previous section have shown that an equatorial outflow produces double-peaked line profiles, we can speculate that the disk material is not revolving on stable Keplerian but rather on slightly outwards spiraling orbits.

Testing this hypothesis revealed that to reproduce the  $\lambda 5577$  line profile we need to include an additional outflow velocity at the inner edge of the [O I] line forming region of  $v_{\text{out}} = (9.0 \pm 0.5) \text{ km s}^{-1}$ . The resulting line profile is shown as the dashed line fit to the  $\lambda 5577$  line in the lower panel of Fig. 9.

**Table 4.** Best-fit parameters of the two competing scenarios for S 65.

Parameter	Outflowing disk		Keplerian disk	
	$R_{\text{in}}$	$R_{\text{out}}$	$R_{\text{in}}$	$R_{\text{out}}$
$r[R_{\odot}]$	1	$\geq 400$	$\sim 90$	$\sim 3000$
$v_{\text{outflow}} [\text{km s}^{-1}]$	$22 \pm 1.0$	$16 \pm 1.0$	$9 \pm 0.5$	$\leq 2.0$
$v_{\text{rot}} [\text{km s}^{-1}]$	—	—	$30 \pm 1.0$	$5 \pm 0.5$
$v_{\text{turb}} [\text{km s}^{-1}]$	$8 \pm 0.5$	$11 \pm 0.5$	—	—
$n_{\text{e}}(r) [\text{cm}^{-3}]$	$1.2 \times 10^9$	$< 7.6 \times 10^3$	$8.2 \times 10^6$	$7.4 \times 10^3$

On the other hand, the profiles of the lines  $\lambda\lambda 6300, 6364$ , which are formed at a much larger distance, are not compatible with such an outflow component. In principle no outflow is needed for these lines, but an outflow component of  $v_{\text{out}} \lesssim 2 \text{ km s}^{-1}$  would still reproduce the profiles reasonably well, indicating a slow-down of the outflow.

If the observed [OI] lines result indeed from a Keplerian (or quasi-Keplerian) rotating disk, the question arises whether this disk extends down to the stellar surface, or whether the material is detached from the stellar surface. If the disk extends down to (or close to) the stellar surface, the disk parts within  $90 R_{\odot}$ , from which no contribution to the [OI] emission is seen, should consequently be ionized. Because ionized oxygen is also known to have forbidden emission lines in the optical spectral range, we calculated the expected line luminosity and profile for the strongest of these lines, which is usually the [OII]  $\lambda 7319$  line, arising in the inner disk parts that extends from the stellar surface out to  $90 R_{\odot}$ . The resulting line profile and intensity are then compared to the weakest of our [OI] lines, i.e., the  $\lambda 5577$  line. This comparison is shown in Fig. 10. The [OII] line turns out to be much broader (due to the higher rotation velocities closer to the star) and about five times more intense than the  $\lambda 5577$  line. Therefore it should be clearly detectable. But our spectra do not show indications for the presence of any [OII] line. This could indeed indicate that if the Keplerian rotating disk scenario is the correct one, the material must be detached from the star.

## 4. Discussion

### 4.1. Outflowing versus Keplerian rotating disk

So far, modeling of the [OI] line luminosities and profiles alone did not allow us to unambiguously distinguish between the outflowing and the Keplerian rotating disk model. Both can provide a plausible scenario for the neutral material around S 65, and we summarized the best-fit model parameters for each in Table 4. The question thus arises whether we can find additional, predominantly kinematical hints in our data that would allow us to favor one of the disk models.

Besides the [OI] lines, our spectra display clearly double-peaked line profiles of the [CaII] lines (see Fig. 4). The measured velocities and equivalent widths are listed in Table 5. The observed line ratio [CaII]  $\lambda 7291/\lambda 7324$  of  $1.45 \pm 0.13$  does not give a conclusive hint for the formation region of these lines, but agrees more with the formation in the low-density limit (1.495) rather than in the high-density limit (1.535). These values have been determined and discussed in detail by Hartigan et al. (2004), and the critical density is  $\sim 5 \times 10^7 \text{ cm}^{-3}$ .

The measured peak and *FWHM* velocities are very similar to the values found for the [OI]  $\lambda 5577$  line, indicating that the [CaII] lines originate from the same region. In both disk scenar-

**Table 5.** Velocities obtained from the peak separation and the *FWHM* values, and equivalent widths of the [CaII] emission lines.

$\lambda$ [Å]	$v_{\text{peaks}}$ [km s <sup>-1</sup> ]	$v_{\text{FWHM}}$ [km s <sup>-1</sup> ]	<i>EW</i> [Å]
7291	$42.0 \pm 2$	$55.2 \pm 2$	$3.04 \pm 0.21$
7324	$38.6 \pm 2$	$56.8 \pm 2$	$2.09 \pm 0.11$

ios the electron density in the [OI] line formation regions are the same, i.e., in the region of the [OI]  $\lambda 5577$  line formation it ranges from  $n_{\text{e}} = 8.0 \times 10^6 \dots 1.5 \times 10^6 \text{ cm}^{-3}$ , while it is much lower within the [OI]  $\lambda\lambda 6300, 6364$  line formation region, extending over  $n_{\text{e}} = 5.0 \times 10^5 \dots 7.5 \times 10^3 \text{ cm}^{-3}$ . Consequently, the [CaII] lines are indeed formed below the critical density as expected from the measured line ratio. Although the kinematics derived from the [CaII] lines cannot help to distinguish between the outflowing and the Keplerian rotating disk we emphasize that the intense and clearly double-peaked [CaII] lines seen in the spectrum of S 65 provide an additional strong indication for the existence of a gaseous disk.

Nevertheless, we think that the Keplerian rotating disk is the more reasonable scenario. Supporting kinematical arguments in favor of the Keplerian disk are given by: (i) the symmetric, unshifted forbidden emission lines and (ii) the sharp absorption components.

We measured the *FWHM* velocities of all unblended forbidden emission lines. The velocities of all lines are very similar, resulting in a mean value of  $(37.09 \pm 4.16) \text{ km s}^{-1}$ . This value is slightly lower than the *FWHM* velocities of the [OI]  $\lambda\lambda 6300, 6364$  lines, indicating that the bulk of forbidden emission lines originates in regions near but beyond (i.e. at larger distances and hence lower velocities than) the [OI] lines. This scenario is difficult to explain with an outflowing disk model, especially because that model requires an increase in turbulent velocity with distance from the star. On the other hand, it is logical to explain the profiles of the forbidden emission lines with the Keplerian disk model. The symmetric line profile with no peak separation means that the emission is formed over a large disk, as for the [OI]  $\lambda\lambda 6300, 6364$  lines, but extending to distances at which the rotation is too small ( $< 5 \text{ km s}^{-1}$ ) for the peaks to be still separated.

Even stronger support for the Keplerian disk scenario is given by the numerous shell lines, i.e., the emission lines with a sharp absorption component reaching below the stellar undisturbed flux. As for classical Be shell stars (e.g., Porter & Rivinius 2003), we can use these sharp absorption components to extract the information on the radial velocity structure, because these lines involve absorption of the photospheric flux throughout the whole disk. The wavelength displacements of the absorption components with respect to the line center of the emission line together with the measured widths of the absorption components deliver information about the kinematics of the absorbing medium, i.e., the kinematics of the disk.

For all the unblended emission lines with pronounced absorption components we measured the central wavelengths and the *FWHM* values of their absorption components. The central wavelengths of the absorption components were corrected for the systemic velocity. The velocities resulting from their *FWHM* values are plotted in Fig. 11 versus their velocity offsets of their central wavelengths, defined by the difference  $v_{\text{obs}} - v_{\text{sys}}$ . From this plot we can draw the following conclusions: Firstly,

all absorption components are blueshifted, meaning that those disk parts in which the absorption happens show a slow outflow ranging from 0 to about  $5 \text{ km s}^{-1}$ . These low outflow velocities agree well with those found for the Keplerian disk scenario (see Table 4). Secondly, the  $FWHM$  velocities of the absorption components range from about 6 to about  $13 \text{ km s}^{-1}$ . Interpreting them with the rotation velocity of the disk, the bulk of the absorption happens at rotation velocities between about 3 and  $6.5 \text{ km s}^{-1}$ . In addition, there seems to be a slight trend (but this trend might also be spurious and caused by a few outliers) towards slower outflow for lower rotation velocities as indicated by the dashed line, which represents the linear regression calculated for the data points. In that respect it is also interesting to note that this trend is also seen when comparing the results for Fe II with those of the (though rare) Fe I lines. The latter are concentrated in the right part of the plot, i.e., at the region with lower outflow and lower rotation velocities, which is logical, because we expect an outwards decreasing ionization structure in the disk.

A further point that needs to be discussed is the inclination of the system. All our conclusions presented so far are based on an assumed edge-on orientation of the system. As discussed in Sect. 3.2 the derived projected rotation velocity is not conclusive and can only be considered as a lower limit to the real projected velocity. Even if we request the star to rotate at its critical limit (see Sect. 4.2 below), we cannot claim that the inclination then has to follow from  $i = \arcsin(v_{\text{rot}}/v_{\text{crit}}) = \arcsin(0.75) = 48.6^\circ$ , but it can have any value between  $48.6^\circ$  and  $90^\circ$ . On the other hand, as mentioned in Sect. 3.1, the numerous shell lines speak in favor of a system viewed more or less edge-on. With a total opening angle for B[e] supergiant stars' disks of  $\sim 20^\circ$  (see Sect. 3.3.1), a minimum inclination of about  $\sim 80^\circ$  might still be possible for the line-of-sight to pass through the disk material. In this case, the difference in velocity compared to a completely edge-on orientation is negligible. Yet we have to admit that this argument only holds if the disk maintains its constant opening angle, i.e. if its outer parts are not flared. So far nothing is known about the structure and shape (and especially about a possible flaring) of the disks around B[e] supergiants at large distances. Therefore we consider the close to edge-on orientation (i.e.  $i \gtrsim 80^\circ$ ) used in our model as a plausible scenario.

Although the above summarized arguments can only be regarded as qualitative indications rather than real proofs, they nevertheless seem to speak in favor of a Keplerian disk scenario. What remains to be discussed is therefore the problem of the origin of such a disk.

#### 4.2. Possible disk formation mechanism

The source S 65 is in an evolved evolutionary phase of an early-type progenitor star, with an initial mass of  $35 \dots 40 M_\odot$ . Hydrodynamic calculations for a  $35 M_\odot$  star by García-Segura et al. (1996b) have shown that due to its high mass-loss rate and wind speed during its main-sequence evolution, the stellar wind deposits sufficient energy into the surrounding medium to sweep up the circumstellar matter into a so-called interstellar (or main-sequence) bubble. When entering the supergiant phase, this bubble has grown in size up to a radius of about  $35 \dots 40 \text{ pc}$  (García-Segura et al. 1996b). Consequently, the disks seen around B[e] supergiants with sizes of only a few hundred to a few thousand AU cannot be pre-main sequence in origin.

In single-star evolution, the disk-formation mechanism in evolved massive stars is not well understood (for a review see, e.g., Owocki 2006). However, as first noted by Struve (1931) rapid (critical) stellar rotation seems to play the key role. Studies

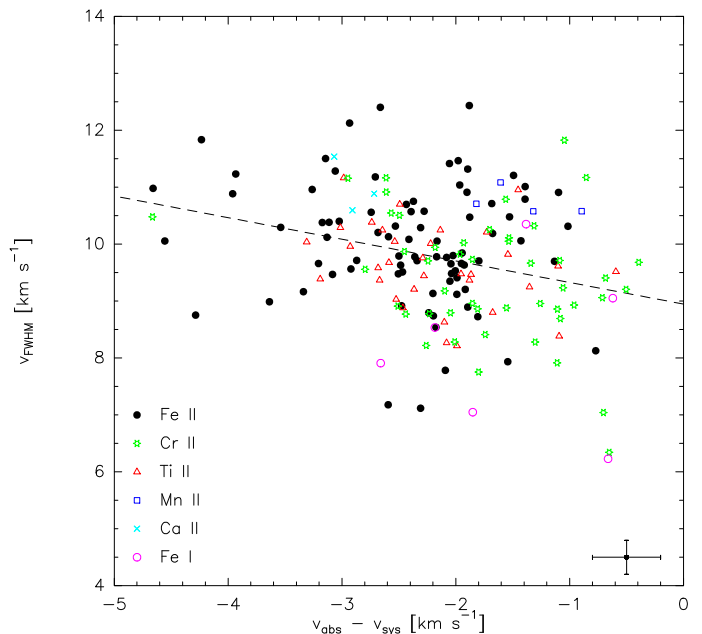


**Fig. 11.**  $FWHM$  velocities versus central peak velocities of the sharp absorption components. Errors in velocities are indicated by the cross in the lower right corner. The dashed line indicates the result from a linear regression.

on disk formation around the most rapidly rotating stars known, i.e., the classical Be stars, revealed that their disks are most probably driven by viscosity (see, e.g., Porter 1999, Okazaki 2001, Jones et al. 2008), resulting in quasi-Keplerian rotating disks with a slow (few  $\text{km s}^{-1}$ ) equatorial outflow component, in agreement with observations (Clark et al. 2003). The star S 65 also seems to be rotating (close to) critical. Consequently, only a slight perturbation, perhaps in form of stellar pulsations (Owocki 2006), would be sufficient to launch matter into orbit and to initiate a viscously driven disk. The kinematics found for the disk of S 65 seem to agree with a quasi-Keplerian disk with a low outflow velocity.

Other possibilities for disk formation would usually require a close companion, which cannot efficiently accrete the material transferred from the primary so that an accretion disk would form. The best known example for this mass transfer and disk-formation process in a massive evolved system is certainly  $\eta$  Car (e.g. Soker 2003). But though studied for decades, none of the B[e] supergiants has so far been reported to have a close companion (e.g. Kraus et al. 2010). In addition, neither the spectral energy distribution of S 65 nor our high-quality spectra, which have been taken on different dates covering observing periods as long as 11 years and as short as 24 hours, show any indication for a companion. Also, our spectra show no evidence for ongoing accretion. Although the existence of a companion cannot definitely be ruled out, we consider it as the less probable scenario for the disk formation around S 65.

Whether the disk around S 65 is indeed driven viscously, as suggested by the observed (quasi-)Keplerian rotation and the slow outflow component, needs to be studied in a future work. Also, whether the disk indeed slows down from inside out as suggested by our data, is an interesting question that needs to be investigated in much more detail than can be done here.

#### 4.3. The connection with LBVs

Another still unsolved problem is related to the question whether B[e] supergiants are a special evolutionary phase in single-star evolution through which only massive stars with very specific initial conditions will evolve, or whether all massive stars have to go through the B[e] supergiant phase. And if the latter is true, then what are the direct progenitors/descendants of the B[e] supergiant phase ?

B[e] supergiants are often discussed in connection with Luminous Blue Variables (LBVs). This is certainly because LBVs also show an indication for a disk or ring structure of circumstellar material. Although a bipolar or multipolar structure seen in several LBVs like in  $\eta$  Car can be caused by binary interaction (Soker 2003), the majority of LBVs have not been reported to have a close companion. Instead, their often seen ring-shaped nebulae (e.g., Nota et al. 1995) can easily be explained by wind-wind interaction in single-star evolution (García-Segura et al. 1996a). Morphological studies of LBV nebulae imply that the slow and dense wind arises mainly from the equatorial regions (Nota et al. 1995). And as for the B[e] supergiants, rapid stellar rotation is thought to play a major role in triggering this non-spherical mass-loss.

The second common characteristic is related to the outflow velocity. Weis (2003) studied the kinematics of LBV nebulae and found that their expansion velocities seem to decrease with metallicity. The LBV nebulae in the SMC are thus expected to have expansion velocities of less than  $10 \text{ km s}^{-1}$ ; hence S 65 with its outflow component of a few  $\text{km s}^{-1}$  would fit in perfectly. With regard to this, we add that for the B[e] supergiant R 126 in the LMC a disk outflow velocity of  $\sim 11.5 \text{ km s}^{-1}$  was determined (Kraus et al. 2007), in good agreement with the outflow velocities of LBV nebulae in the LMC. We also find that the gas masses in the disks around S 65 ( $\gtrsim 1.5 \times 10^{-2} M_{\odot}$ ) and R 126 ( $\gtrsim 6 \times 10^{-2} M_{\odot}$ ) fit nicely to the range of gas masses found for LBV nebulae (Nota et al. 1995; Weis 2003).

The last common characteristic refers to the stellar rotation speed. Groh et al. (2009) recently found for two of the Galactic LBVs, AG Car and HR Car, rotation velocities during their visual minimum phase in excess of 85% of their critical velocity. Hence Groh et al. (2009) defined an LBV minimum-instability strip, which indicates the position in the HR diagram at which critical rotation for LBVs is expected. This is shown in Fig. 12. To the left of the instability strip is the physically unstable region for LBVs, labeled with  $v_{\text{rot}}/v_{\text{crit}} > 1$ . We also included the position of S 65 into this plot. Its location is in the valid range for LBVs, but also very close to the instability strip.

In summary, the rapid rotation, the close vicinity in the HR diagram to the LBVs and the LBV minimum instability strip, as well as the similar disk mass and outflow velocity derived for S 65 might all hint towards a connection between LBVs and S 65 (or perhaps B[e] supergiants in general). The most logical conclusion is thus that S 65 is currently in the LBV visible minimum phase, after experiencing one (or more) eruptions, in which a large amount of material was ejected from the rapidly rotating star, predominantly in equatorial direction, which formed the Keplerian ring or disk-like structure. If this scenario is correct, then S 65 could be in a state just before the new, fast wind sets in, which will compress the disk/ring material into the typical LBV nebula. The signatures of Keplerian rotation, as still seen in the disk of S 65, might disappear during this wind compression process, because the material will be radially accelerated outwards.

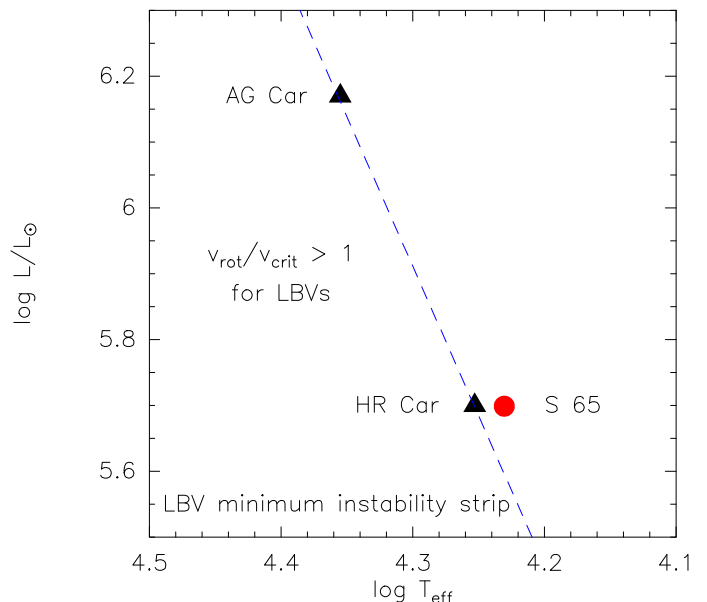


**Fig. 12.** Location of S 65 within the HR diagram and with respect to two rapidly rotating Galactic LBVs close to the LBV minimum instability strip (after Groh et al. 2009). For details see text.

We cannot conclusively answer whether S 65 indeed belongs to the class of LBVs, especially because a star is called an LBV only after a giant eruption and the typical S Dor variability has been recorded. Nevertheless, there is ample evidence that S 65 shares several of the major LBV characteristics.

## 5. Conclusions

We studied the circumstellar material of the rapidly rotating SMC B[e] supergiant star S 65. The sharp absorption components seen in its numerous emission lines indicate a high-density disk viewed almost edge-on. Surprisingly, the spectrum also displays two very intense and clearly double-peaked [CaII] lines, supporting the high-density gaseous disk hypothesis. Based on the modeling of both, the observed line luminosities of the [OII] lines and their line profiles, we found that the disk around the B[e] supergiant S 65 must be predominantly neutral in hydrogen. The total amount of ionized hydrogen is found to be less than  $\sim 0.1\%$ , and the total amount of gas traced within the [OII] line-forming region is  $\sim 1.5 \times 10^{-2} M_{\odot}$ . In combination with the kinematical information provided by the numerous lines, our model results favor the interpretation of a detached (quasi-)Keplerian rotating disk rather than an outflowing disk. The location of S 65 in the HR diagram places the star close to the recently defined LBV minimum instability strip. Together with its high rotation velocity close to the critical limit and its large amount of slowly expanding circumstellar material similar to that seen for LBV nebulae, it seems that S 65 might be the link between B[e] supergiants and LBVs.

*Acknowledgements.* We thank the referee, Dr. J.H. Kastner, for his valuable comments on the manuscript. This research made use of the NASA Astrophysics Data System (ADS). M.K. acknowledges financial support from GA AV ČR number KJB300030701. M.B.F. acknowledges financial support from the Centre National de la Recherche Scientifique (CNRS) and from the Programme National de Physique Stellaire. M.B.F. also acknowledges Conselho Nacional de Desenvolvimento Científico e Tecnológico (CNPq-Brazil) for the post-doctoral grant.

## References

- Charbonnel C., Meynet G., Maeder A., Schaller, G., & Schaerer, D. 1993, *A&AS*, 101, 415
- Clark, J. S., Tarasov, A. E., & Panko, E. A. 2003, *A&A*, 403, 239
- Curé, M. 2004, *ApJ*, 614, 929
- Curé, M., Rial, D. F., & Cidale, L. 2005, *A&A*, 437, 929
- Dufton, P. L., Ryans, R. S. I., Trundle, C., et al. 2005, *A&A*, 434, 1125
- Feast, M. W., Thackeray, A. D., & Wesselink, A. J. 1960, *MNRAS*, 121, 344
- García-Segura, G., Mac Low, M.-M., & Langer, N. 1996a, *A&A*, 305, 229
- García-Segura, G., Langer, N., & Mac Low, M.-M. 1996b, *A&A*, 316, 133
- Gray, D. F. 1976, *The observation and analysis of stellar photospheres* (New York: Wiley)
- Grevesse, N. & Sauval, A. J., 1998, *Space Sci. Rev.* 85, 161
- Groh, J.H., Damineli, A., Hillier, D.J., et al. 2009, *ApJ*, 705, L 25
- Hanuschik, R. W. 2000, in: *The Be Phenomenon in Early-Type Stars*, ed. M. A. Smith, H. F. Henrichs, & J. Fabregat (San Francisco: ASP), ASP Conf. Ser. Vol. 214, 518
- Hamuy, M., Suntzeff, N. B., Heathcote, S. R., et al. 1994, *PASP*, 106, 566
- Hartigan, P., Edwards, S., & Pierson, R., 2004, *ApJ*, 609, 261
- Jones, C. E., Sigut, T. A. A., & Porter, J. M. 2008, *MNRAS*, 386, 1922
- Kafatos, M., & Lynch, J. P. 1980, *ApJS*, 42, 611
- Kastner, J. H., Buchanan, C. L., Sargent, B., & Forrest, W. J. 2006, *ApJ*, 638, L 29
- Keller, S. C., & Wood, P. R. 2006, *ApJ*, 642, 834
- Kraus, M. 2006, *A&A*, 456, 151
- Kraus, M., & Borges Fernandes, M. 2005, in: *The Nature and Evolution of Disks Around Hot Stars*, ed. R. Ignace & K.G. Gayley (San Francisco: ASP), ASP Conf. Ser. Vol. 337, 254
- Kraus, M., & Lamers, H. J. G. L. M., 2003, *A&A*, 405, 165
- Kraus, M., Borges Fernandes, M., & de Araújo, F. X. 2007, *A&A*, 463, 627
- Kraus, M., Borges Fernandes, M., & Chesneau, O. 2010, in *Binaries, Key to Comprehension of the Universe*, ed. A. Prša & M. Zejda, ASP Conf. Ser., in press
- Kraus, M., Borges Fernandes, M., Kubát, J., & de Araújo, F. X. 2008, *A&A*, 487, 697
- Kraus, M., Borges Fernandes, M., Andrade Pilling, D., & de Araújo, F.X., 2006, in *Stars with the B[e] Phenomenon*, ed. M. Kraus & A.S. Miroshnichenko (San Francisco: ASP), ASP Conf. Ser. Vol. 355, 163
- Lamers, H. J. G. L. M., & Pauldrach, A. W. A. 1991, *A&A* 244, L5
- Maeder, A., & Meynet, G. 2000, *A&A*, 361, 159
- Magalhães, A. M. 1992, *ApJ*, 398, 286
- Magalhães, A. M., Melgarejo, R., Pereyra, A., & Carciofi, A. C. 2006, in *Stars with the B[e] Phenomenon*, ed. M. Kraus & A. S. Miroshnichenko (San Francisco: ASP), ASP Conf. Ser., 355, 147
- Maurice, E. 1976, *A&A*, 50, 463
- McGregor, P. J., Hillier, D. J., & Hyland, A. R. 1988a, *ApJ*, 334, 639
- McGregor, P. J., Hyland, A. R., & Hillier, D. J. 1988b, *ApJ*, 324, 1071
- McGregor, P. J., Hyland, A. R., & McGinn, M. T. 1989, *A&A*, 223, 237
- Melgarejo, R., Magalhães, A. M., Carciofi, A. C. & Rodrigues, C. V. 2001, *A&A*, 377, 581
- Mendoza, C. 1983, *IAU Symp.*, 103, 143
- Meynet, G., & Maeder, A. 2005, *A&A*, 429, 581
- Morris, P. W., Eenens, P. R. J., Hanson, M. M., Conti, P. S., & Blum, R. D. 1996, *ApJ*, 470, 597
- Nota, A., Livio, M., Clampin, M., & Schulte-Ladbeck, R., 1995, *ApJ*, 448, 788
- Muratorio, G. 1981, *A&AS*, 43, 111
- Okazaki, A. T. 2001, *PASJ*, 53, 119
- Owocki, S.P. 2006, in *Stars with the B[e] Phenomenon*, ed. M. Kraus & A. S. Miroshnichenko (San Francisco: ASP), ASP Conf. Ser., 355, 219
- Pelupessy, I., Lamers, H. J. G. L. M., & Vink, J.S. 2000, *A&A* 359, 695
- Porter, J. M. 1999, *A&A*, 348, 512
- Porter, J. M. 2003, *A&A*, 398, 631
- Porter, J. M., & Rivinius, Th. 2003, *PASP*, 115, 1153
- Prévot, M. L., Lequeux, J., Maurice, E., et al. 1984, *A&A*, 132, 389
- Soker, N. 2003, *ApJ*, 597, 513
- Stahl, O. 2001, in *Eta Carinae & Other Mysterious Stars* ed. T. Gull, S. Johansson & K. Davidson (San Francisco: ASP), ASP Conf. Ser., 242, 163
- Steffen, M., & Schönberner, D. 2003, in *Planetary Nebulae: Their Evolution and Role in the Universe*, ed. S. Kwok, M. Dopita, & R. Sutherland (San Francisco: ASP), IAU Symp. Vol. 209, 439
- Störzer, H., & Hollenbach, D. 2000, *ApJ*, 539, 751
- Struve, O. 1931, *ApJ*, 73, 94
- Townsend, R.H.D., Owocki, S.P., & Howarth, I.D., 2004, *MNRAS*, 350, 189
- Weis, K., 2003, *A&A*, 408, 205
- Wiese, W. L., Smith, M. W., & Glennon, B. M. 1966, *Atomic Transition Probabilities, Vol. 1* (National Standard Reference Data System, Washington D.C.)
- Zickgraf, F.-J. 1989, in *Physics of Luminous Blue Variables*, ed. K. Davidson, A. F. J. Moffat, & H. J. G. L. M. Lamers (Dordrecht: Kluwer Academic Publishers), IAU Colloquium 113, 117
- Zickgraf, F.-J. 2000, in *The Be Phenomenon in early-type stars*, ed. M. A. Smith, H. F. Henrichs, & J. Fabregat (San Francisco: ASP), ASP Conf. Ser., 214, 26
- Zickgraf, F.-J., Wolf, B., Stahl, O., Leitherer, C., & Klare, G. 1985, *A&A*, 143, 421
- Zickgraf, F.-J., Wolf, B., Stahl, O., Leitherer, C., & Appenzeller, I. 1986, *A&A*, 163, 119
- Zickgraf, F.-J., Wolf, B., Stahl, O., & Humphreys, R. M. 1989, *A&A*, 220, 206